

Article

Late Cretaceous Tectono-Metamorphic Events in the Skyros Upper Metamorphic Unit (Olympus Mountain), Aegean Sea, Greece

Dimitra Boundi ¹, Dimitrios Papanikolaou ¹, Giulia Bosio ²  and Chiara Montemagni ^{2,*} 

¹ Department of Geology and Geoenvironment, National and Kapodistrian University of Athens, 15784 Athens, Greece; dboudi@geol.uoa.gr (D.B.); dpapan@geol.uoa.gr (D.P.)

² Department of Earth and Environmental Sciences, University of Milano-Bicocca, 20126 Milano, Italy; giulia.bosio@unimib.it

* Correspondence: chiara.montemagni@unimib.it

Abstract: Late Cretaceous metamorphic events are known in Crete and the Cyclades from klippen above the External Hellenides. This work extends their occurrence to the North Aegean area within the tectonic units of the Internal Hellenides. New ⁴⁰Ar/³⁹Ar white mica ages from garnet-bearing micaschists of the Upper Metamorphic Unit of Skyros Island, cropping out in the Skyrian Olympus Mountain, document a Late Cretaceous tectono-metamorphic evolution. Several mica generations have been distinguished using electron probe microanalyses and were dated using the ⁴⁰Ar/³⁹Ar method: a relict mica older than 96 Ma, followed by a foliation-forming mica of about 88–84 Ma and alteration phases ≤ 68 Ma were recognized. This Cretaceous tectono-metamorphic evolution falls between the closure of the internal Axios/Vardar oceanic basin in the Late Jurassic–Early Cretaceous, and the closure of the external Pindos–Cyclades oceanic basin in the Early Cenozoic. The position of the Upper Metamorphic Unit of Skyros was probably within the evolving Hellenic volcanic/magmatic arc during the continuous subduction of the African plate beneath the European plate. The present tectonic position of the units bearing the Late Cretaceous metamorphic event is the result of the Cenozoic tectonic emplacement onto the more external units across the Hellenides from the Pelagonian to the Pindos–Cyclades domain.

Keywords: External Hellenides; Internal Hellenides; Skyros; ⁴⁰Ar/³⁹Ar dating; Late Cretaceous; metamorphism



Citation: Boundi, D.; Papanikolaou, D.; Bosio, G.; Montemagni, C. Late Cretaceous Tectono-Metamorphic Events in the Skyros Upper Metamorphic Unit (Olympus Mountain), Aegean Sea, Greece.

Geosciences **2024**, *14*, 69. <https://doi.org/10.3390/geosciences14030069>

Academic Editors: Olivier Lacombe and Jesus Martinez-Frias

Received: 14 December 2023

Revised: 1 March 2024

Accepted: 3 March 2024

Published: 5 March 2024



Copyright: © 2024 by the authors. Licensee MDPI, Basel, Switzerland. This article is an open access article distributed under the terms and conditions of the Creative Commons Attribution (CC BY) license (<https://creativecommons.org/licenses/by/4.0/>).

1. Introduction

The Hellenides comprise a segment of the Tethyan Alpine Orogenic Belt that developed along the active European margin during plate convergence between the Eurasian plate in the north and the African plate in the south. Oceanic subduction of the Tethyan basins alternating with continental subduction of intermediate continental terranes with shallow-water carbonate platforms occurred throughout the Late Mesozoic–Cenozoic underneath the European margin [1–5]. The terrane accretion at the southern European margin is sometimes subdivided into discrete events indicated with local names: Cimmerian orogeny (Late Triassic–Lias), observed mainly in the North Aegean Islands of Lesbos and Chios, Paleo-Alpine orogeny (Late Jurassic–Early Cretaceous), observed in the eastern part of the Hellenides, known as the Internal Hellenides, and main Alpine orogeny (Eocene–Oligocene) observed all over the Hellenides, both Internal and External [2–4,6,7]. The main distinction between the Internal and the External Hellenides was based on the existence of the Late Cretaceous unconformity over the paleo-tectonized units in the Internal Hellenides, contrary to the continuous stratigraphic sequences of the External Hellenides from the early Mesozoic to the Eocene–Oligocene [1,8–11]. The absence of tectono-metamorphic events recorded by the Upper Cretaceous–Eocene transgressive sediments of the Internal Hellenides indicates that (1) the Alpine deformation during the Eocene–Oligocene was

restricted to the upper tectonic levels of the crust, comprising mainly thrusting and folding; and (2) the tectono-metamorphic events described in the underlying paleo-tectonized Triassic–Jurassic formations were pre-Late Cretaceous [6,8–10,12]. On the contrary, Alpine tectono-metamorphic events have been observed during the Eocene–Oligocene in the External Hellenides within the medial metamorphic belt in the Olympus–Pelion–Cyclades tectonic windows [13–15] and younger events of late Oligocene–Miocene age have been reported from the external metamorphic belt of Peloponnese–Crete [16,17]. Thus, the Late Cretaceous period corresponds to a gap between the Paleo-Alpine and the Alpine tectonic events in the Hellenides. Nevertheless, some sparse outcrops of small tectonic units reported from Crete and the Cyclades are characterized by Late Cretaceous tectono-metamorphic events, occurring above the External Hellenides nappe pile [17–24] (see inset map of Figure 1).

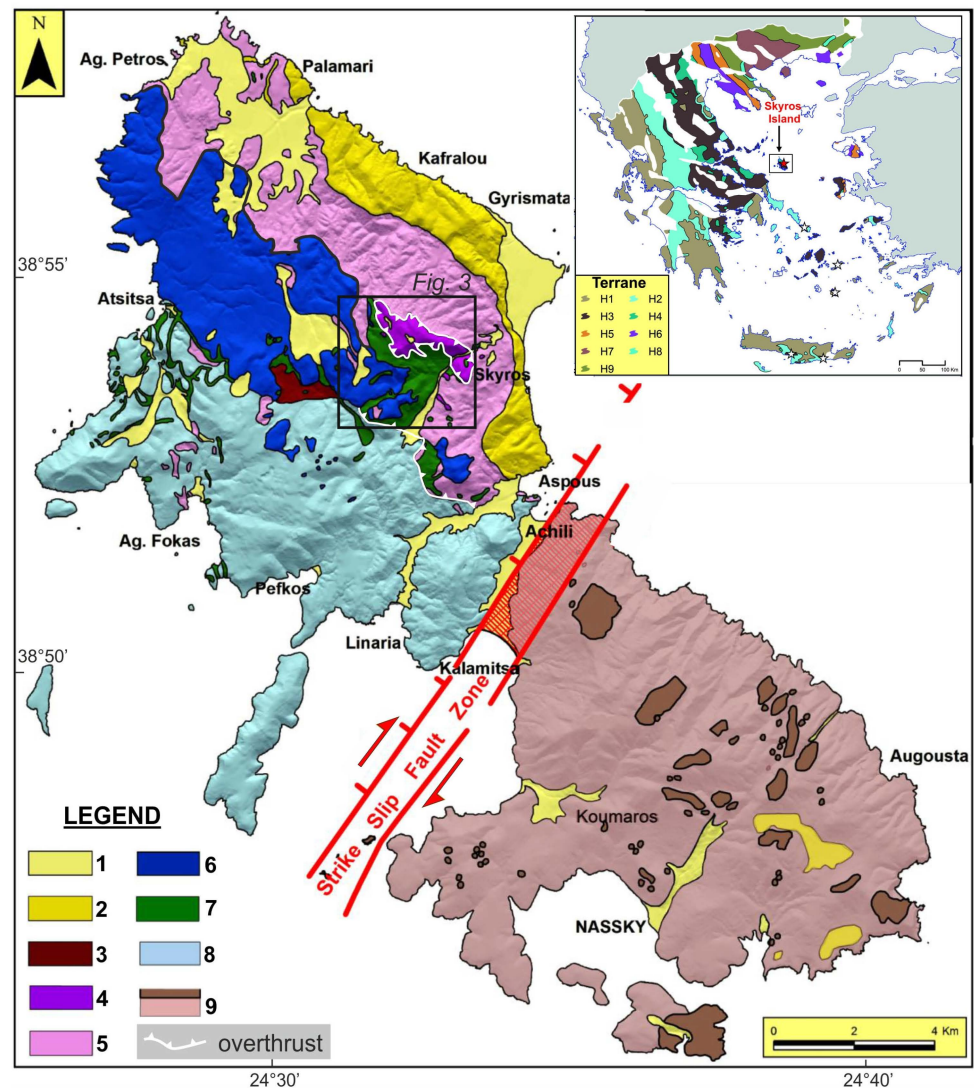


Figure 1. Simplified and modified geological map of Skyros Island based on [25]. 1. Quaternary sediments, 2. Upper Miocene–Lower Pliocene sediments, 3. Miocene volcanics, 4. Upper Metamorphic Unit (UMU) of Skyros, 5. Lower Metamorphic Unit (LMU) of Skyros, 6. Upper Cretaceous Limestones and Flysch, 7. Axios ophiolites (Jurassic), 8. Sub-Pelagonian Unit of NW Skyros. Triassic–Jurassic carbonate platform overlying Permian–Triassic sedimentary sequence, 9. Sub-Pelagonian Unit of SE Skyros. Upper Cretaceous limestones transgressive on the Triassic–Jurassic Carbonate platform and overlying the Permian–Triassic volcano-sedimentary sequence. Inset map: geotectonic Terrane Map of Greece. H1: External Carbonate Platform, H2: Pindos–Cyclades Ocean, H3: Internal

Platform, H4: Axios/Vardar Ocean, H5: Lesvos–Paikon Platform, H6: Lesvos–Circum Rhodope Ocean, H7: Pangeon Platform, H8: Volvi–Eastern Rhodope Ocean, H9: Allochthonous Pre-Alpine Basement of Rhodope [1]. The position of Skyros Island is indicated. The previously known localities with Upper Cretaceous tectono-metamorphic events in H2 are indicated by white stars and the new locality in H4 by a red star. The study area is highlighted with a black box.

In this study, we present new $^{40}\text{Ar}/^{39}\text{Ar}$ data suggesting Late Cretaceous tectono-metamorphic events on Skyros Island, in the NW Aegean Sea. The new data come from the Upper Metamorphic Unit (UMU) of Skyros, cropping out in the Olympus Mountain. The UMU overlies the Lower Metamorphic Unit (LMU) and the relative autochthon Sub-Pelagonian Unit of eastern Greece [25]. Thus, the occurrence of the Late Cretaceous tectono-metamorphic events is extended also in the North Aegean Sea within the Internal Hellenides domain beyond the previously known outcrops within the External Hellenides domain in Crete and the Cyclades.

2. Geological Setting

Skyros Island is bisected by a NE-SW strike slip fault zone [26] separating two neo-tectonic blocks with different geological structures (Figure 1). This fault zone represents the southwestern end of the southern branch of the prolongation of the North Anatolian Fault in the Aegean, passing through the Skyros Basin [27]. The SE block is made up of one monotonous tectonic unit, comprising a Triassic–Jurassic carbonate platform of the Sub-Pelagonian Unit, overlain by underformed transgressive Upper Cretaceous sediments. The NW part comprises several Alpine tectonic units, forming a complex nappe structure with imbrications, indicated by thin interlayers of sheared ophiolite rocks. Additionally, Upper Miocene–Pleistocene sediments crop out along the eastern coastline and a Miocene volcanic outcrop in the central area of the NW part [10,28–33]. The tectonic units of the NW Skyros nappe pile are, from the base to the top (Figure 2):

- (1) A thick Triassic–Jurassic carbonate platform, belonging to the Sub-Pelagonian Unit, stratigraphically overlying a Permian–Triassic volcano-sedimentary sequence of more than 300 m in thickness.
- (2) A thin layer of ophiolite rocks imbricated with thin tectonic wedges of the Triassic–Jurassic platform carbonates. The ophiolite outcrops belong to the Vardar/Axios oceanic basin (H4 in Figure 1) and were tectonically emplaced on top of the carbonate platform (H3 in Figure 1) during Late Jurassic–Early Cretaceous [2,10,30].
- (3) Upper Cretaceous carbonate rocks (Ks) of several hundred meters in thickness, overlain by a flysch. These formations are not metamorphosed and form a tectonic zone of imbrications and tectonic wedges between the underlying Sub-Pelagonian and ophiolite rocks and the overlying metamorphic rocks.
- (4) A wedge-shaped tectonic unit of metamorphic rocks, comprising meta-volcanic rocks, meta-sediments, and pelagic silicate marbles, imbricated with ophiolites. This unit was known as the “Fere-Note” formation [29,33] and was renamed by [10,25] as the “Eo-Hellenic nappe” of Skyros. In fact, it forms the Lower Metamorphic Unit of Skyros (LMU in Figures 2 and 3). Its thickness becomes more than 1 km towards the NE, whereas, towards the SW, it thins out and there are small tectonic wedges/klippen having a thickness of a few tens of meters up to the western coast of Skyros Island.
- (5) On top of all previous tectonic units there is a tectonic klippe of a metamorphic nappe (UMU), forming the highest peak of the Skyrian Olympus Mountain (403 m). This unit was known as the “Skyros tectonic unit” [25] and is here called the Upper Metamorphic Unit of Skyros (UMU in Figures 2 and 3). It comprises pelagic silicate marbles and intercalations of gneisses-schists. Its metamorphic grade is higher than that of the underlying Lower Skyros metamorphic nappe. A strong differentiation of the structural fabric of the Skyros tectonic units is observed with distinction of tectonic structures belonging to the Paleo-Alpine orogenic phase from those of the Alpine orogenic phase [34].

Additionally, a several hundred meters-thick Upper Miocene–Pliocene sedimentary sequence crops out along the northeastern coastline, separated by a NE dipping low-angle extensional detachment fault from the underlying metamorphic rocks of the LMU.

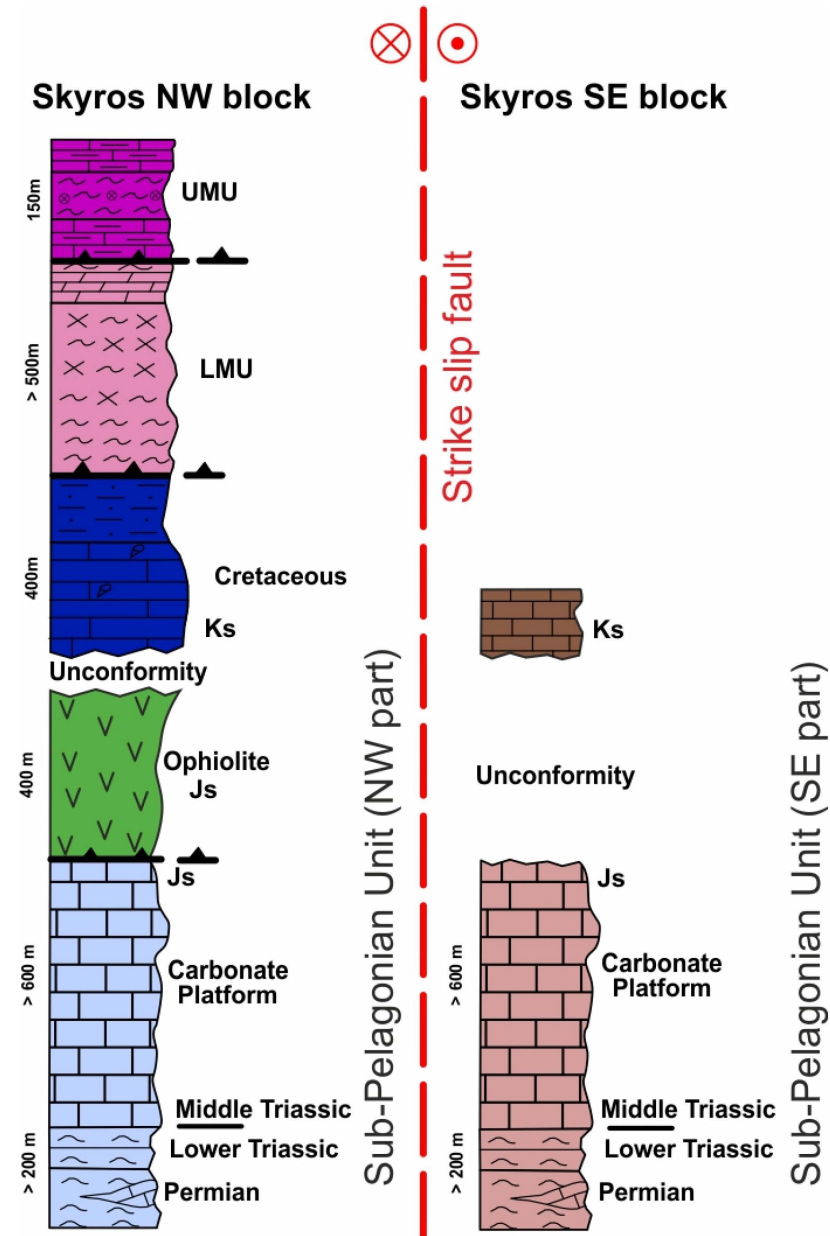


Figure 2. Schematic tectono-stratigraphic columns of the two Skyros blocks, showing the differences between the NW block where two units of metamorphic rocks occur, the UMU and LMU, overlying the relative autochthonous Sub-Pelagonian Unit. This unit comprises the Permian–Lower Triassic volcano-sedimentary cover, overlain by the Middle Triassic–Upper Jurassic carbonate platform and the obducted Axios ophiolites, beneath the Upper Cretaceous limestone and flysch. On the contrary, in the SE block, only the Sub-Pelagonian Unit occurs, made by the lower part of the Permian–Jurassic succession. The top the succession is marked by an unconformity, above which the Upper Cretaceous limestones occur in transgression.

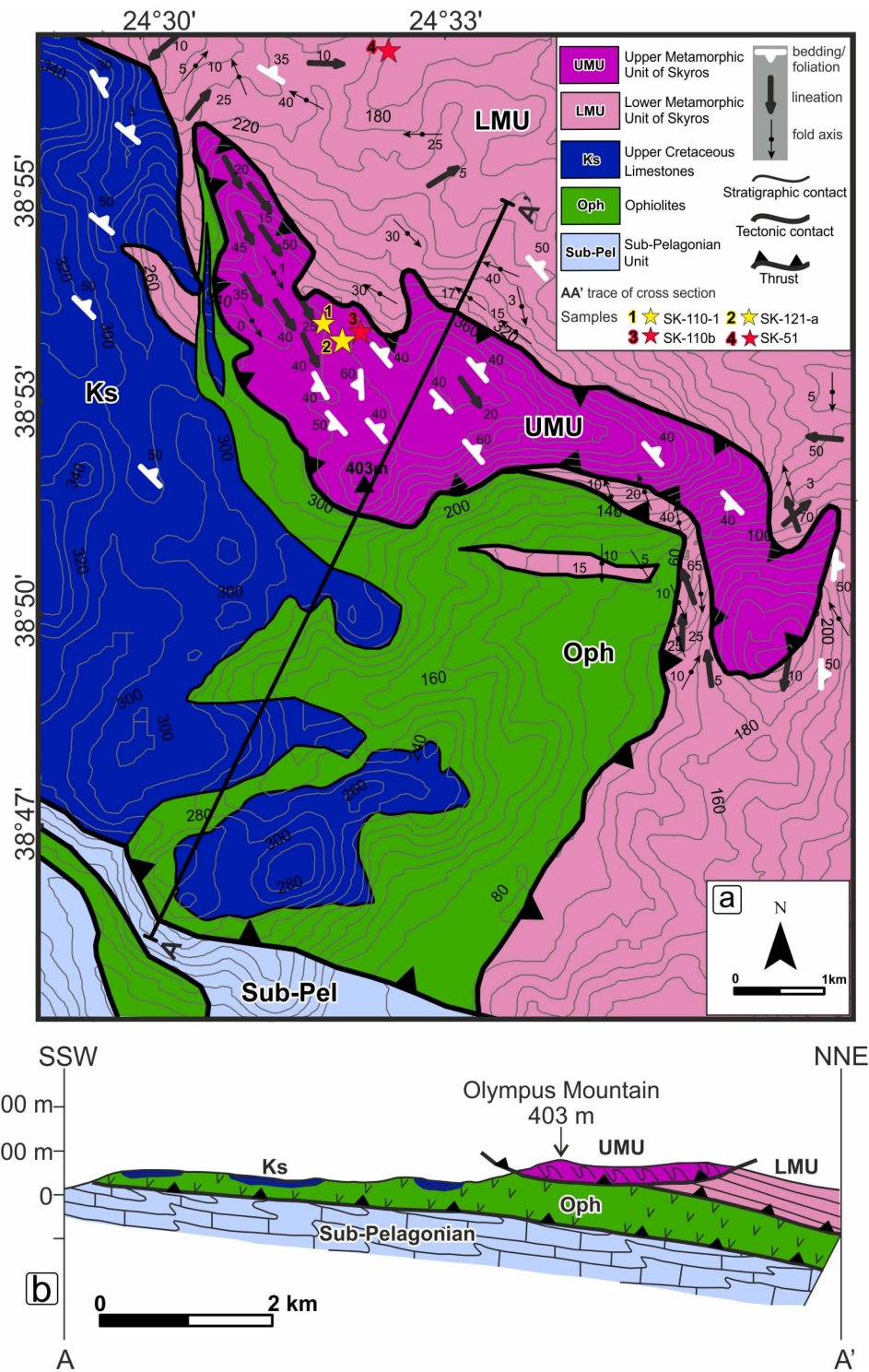


Figure 3. Geological map (a) and geological cross-section (b) of the central part of Skyros Island around the Olympus Mountain. The Upper Metamorphic Unit of Skyros (UMU) is observed above the underlying Lower Metamorphic Unit of Skyros (LMU), the ophiolites (Oph), the Upper Cretaceous carbonates (Ks), and the Sub-Pelagonian Unit (Sub-Pel). The locations of the dated samples SK-110-1 and SK-121-a are shown by yellow stars 1 and 2 and location of samples used for thermobarometry are given by red stars 3 and 4. At depth, the Sub-Pelagonian autochthon unit is represented by the carbonate platform (Tr–J). The thrusts are indicated by a thick black line with barbes and the tectonic contacts without barbes.

3. The Skyros Upper Metamorphic Unit (Olympus Mountain)

3.1. Mesoscale Observations

The UMU of Skyros Island is limited to a single elongate, ca. 5 km long outcrop in the higher mountainous region of Skyros with altitudes between 250 and 400 m (Olympus Mountain has an altitude of 403 m; Figure 3).

It consists of marbles and garnet-bearing micaschists. It forms a klippe with a sub-horizontal tectonic contact, overlying either the LMU of Skyros to the northeast (Figure 4a), or the imbricated thrust sheets of the ophiolites to the southwest (Figure 4b).

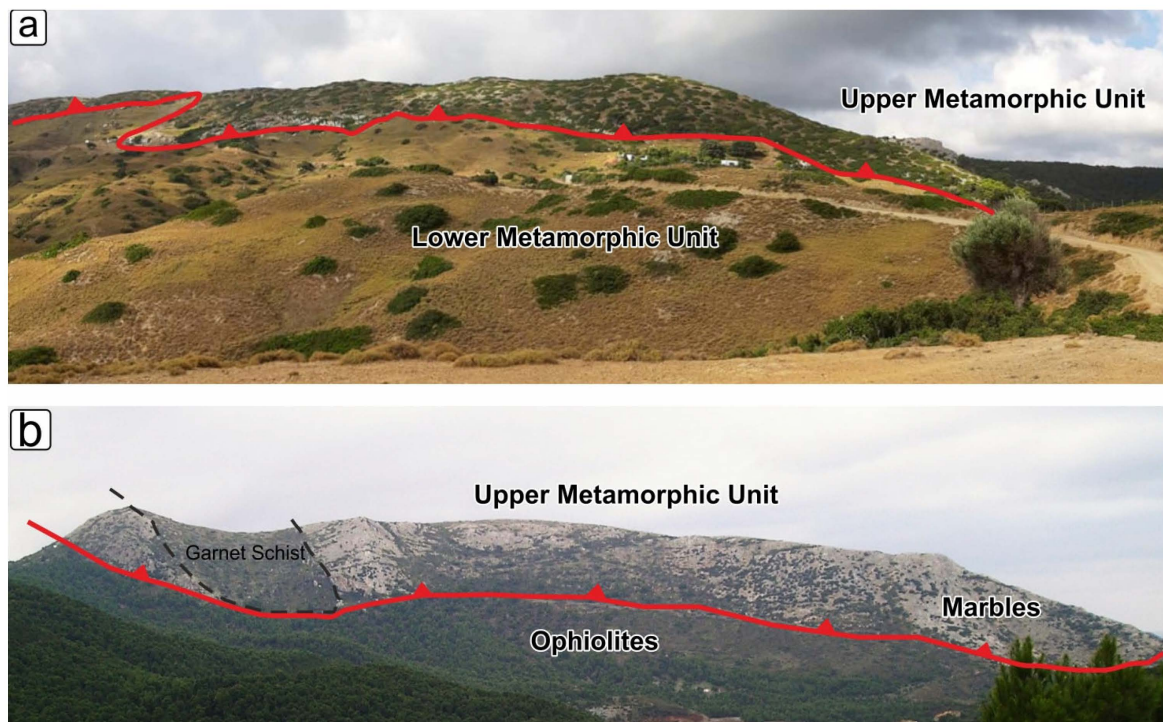


Figure 4. (a) Panoramic view of the UMU of Skyros looking from the east. (b) Panoramic view of the UMU of Skyros looking from the west. The garnet schists form an inclined isoclinal synform between the marbles, whose base is cut by the basal thrust surface. From the east, the UMU is observed to overlie the LMU of Skyros, whereas from the west it overlies the ophiolites.

The marbles form a thick layer having a thickness of more than 150 m within the micaschists, which are observed both overlying and underlying them due to isoclinal folding, as this is also indicated by the occurrence of micaschist in the western part of Olympus Mountain between two marble outcrops (Figure 4b). However, the general structure of the UMU in the Olympus Mountain is characterized by subvertical bedding and schistosity-oriented NW-SE dipping towards the NE. It is remarkable that the marbles are thin-layered pelagic meta-carbonates with abundant siliceous layers, indicating a pelagic-oceanic paleo-environmental domain (Figure 5b). A several meters-thick shear zone comprising cataclastic rocks appears between the marbles of this unit and the underlying ophiolitic rocks (Figure 4b). The micaschists are characterized by a foliation-oriented NW-SE and general dip to the NE and mineral lineations with a dominant NW-SE orientation and plunge to the SE (Figure 5a).

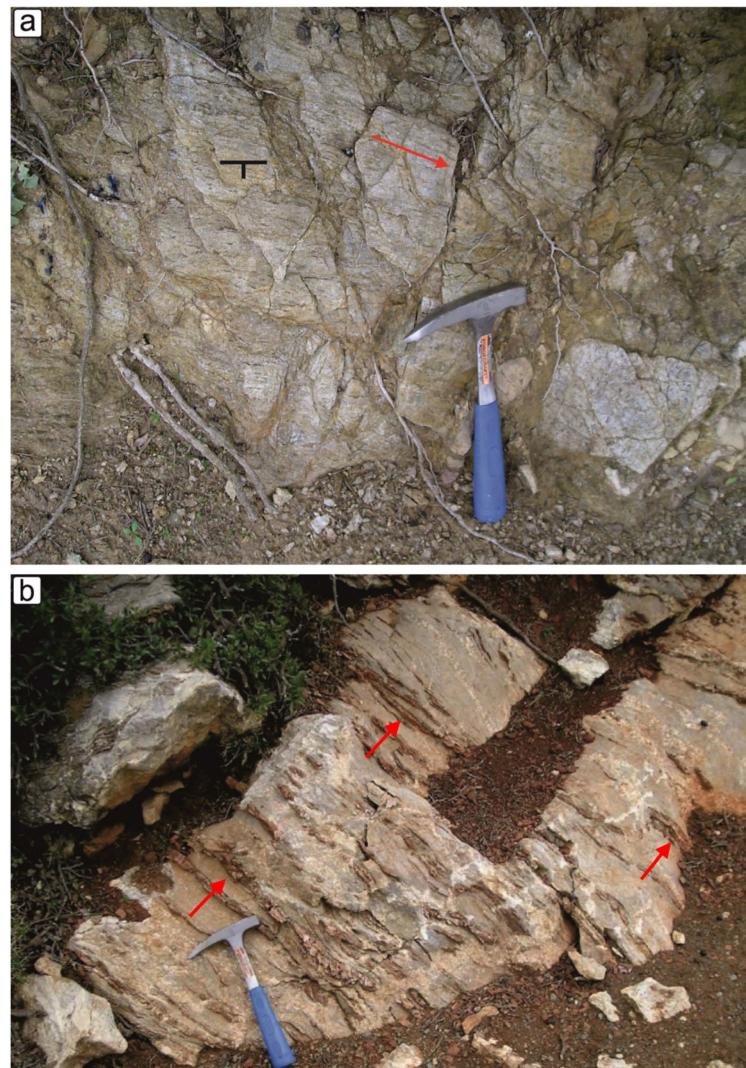


Figure 5. (a) Mineral lineation and foliation on the garnet bearing micaschists of the UMU of Skyros. The red line shows the mineral lineation plunging to the SE. The strike and dip of the foliation is also marked in black. (b) Outcrop appearance of the Pelagic Marbles of the UMU of Skyros showing abundant siliceous layers (indicated by arrows), characterized by their pronounced relief above the adjacent carbonate material.

3.2. Microscale Observations

The peak mineral assemblage of the micaschists (SK-121-a and SK-110-1; Figure 6a–f) comprises garnet, biotite, phengite, quartz, and plagioclase; rutile and titanite occur as accessory minerals. Calcite also occurs in some domains (Figure 6f). Muscovite is recrystallized along the main foliation after HP phengite; chlorite both occurs as relict (Figure 6b) and replaces biotite, forming also coronas around garnet porphyroclasts (Figure 6d).

Almost all micaschist samples consisted of more than 65% muscovite and chlorite, followed by quartz and plagioclase (10%), biotite (5%), garnet (10%), and rutile, titanite and other accessory minerals (10%). The main foliation was defined by muscovite and minor chlorite. Moreover, muscovite and chlorite are present also as relict crystals. The garnet forms porphyroclasts which are enveloped by muscovite forming the main foliation. Garnet, biotite, phengite, chlorite, and rutile predate the main foliation. The quartz recrystallized especially via a bulging recrystallization mechanism.

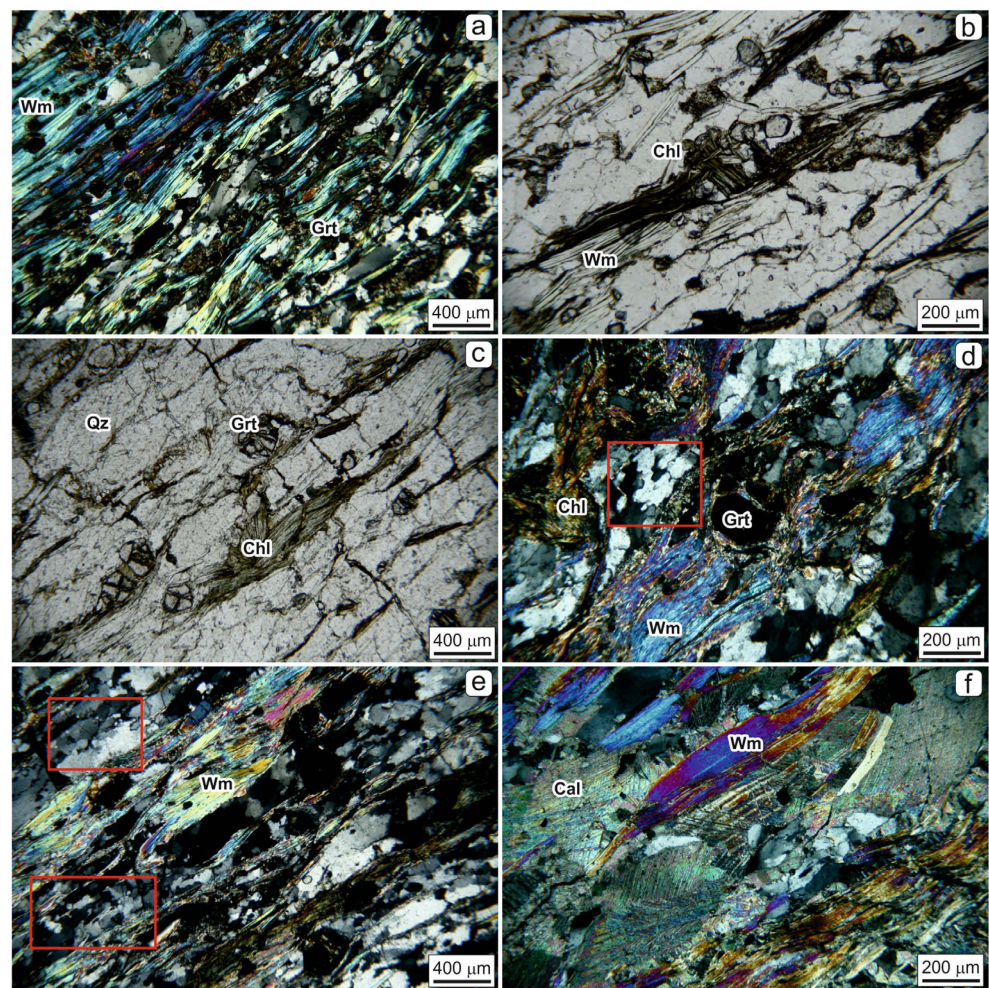


Figure 6. (a) Pervasive main foliation made of muscovite and chlorite and (b) relict chlorite forming a high angle with respect to the main foliation in sample SK-121-a. (c) Muscovite and chlorite forming the main foliation and (d) a garnet porphyroblast enveloped by muscovite in sample SK-110-1. (e) Quartz recrystallized via BLG (red boxes) and muscovite along the main foliation. (f) Calcite occurring in some domains. Mineral abbreviations after [35] except for white mica (Wm).

4. PT Estimation of UMU and LMU

The estimation of the PT conditions of metamorphism was previously conducted [36,37] using the bulk-rock compositions of representative samples from the UMU of Skyros (sample SK-110b, Figure 3) and the LMU of Skyros (sample SK-51, Figure 3). Thus, the local-equilibrium method has been applied successfully only for the Chl-Ph pairs for the LMU of Skyros. The calculated invariant points define the maximum pressure conditions at $P = 11 \pm 1.5$ kbar and $T = 280 \pm 15$ °C; the maximum temperature conditions occur at $T = 384 \pm 13$ °C and $P = 9.2 \pm 0.4$ kbar. One additional chlorite–phengite pair was calculated to be stable at $T = 380 \pm 20$ °C and $P = 7.5 \pm 0.6$ kbar, indicating decompression at a nearly constant temperature. Application of the graphite thermometry revealed an average temperature of 375 ± 25 °C. As such, the maximum temperature (ca. 400 °C) estimated from the graphite thermometer of [38] was in accordance with the maximum temperature estimated from the local equilibria between chlorite and phengite. Hence, along with the calculated T from the Raman spectroscopy of the carbonaceous material method, the peak T conditions are in accordance with the results estimated by the multi-equilibrium method at $P \approx 9.2$ kbar and $T \approx 385$ °C [36,37]. The peak temperature of the UMU of Skyros has been estimated using the PT pseudosection based on the garnet and phengite composition. The petrographic observation of the sample suggests an equilibrium between garnet and

phengitic muscovite. The garnet isopleths converged for the three end-members, and when compared with the observed composition of the garnet indicate $T = 550 \pm 30$ °C at 9.2 ± 1 kbar. The Si-in phengite isopleths are lying between the pressures estimated from the garnet isopleths, suggesting compositional equilibrium with the latter. The estimated temperature should be regarded as the peak one, with the peak assemblage represented by $Wm + Chl + Ph + Bt + Grt + Ep + Rt + Qz + Mt$. The biotite was not observed in the sample, because it has been retrogressed and chloritized [36,37].

5. Analytical Methods

5.1. Petrographic and Microprobe Analyses

Two samples (SK-121-a and SK-110-1) from the micaschists of the UMU of Skyros have been analyzed. Their location is shown in Figure 3 and their geographical co-ordinates are: $38^{\circ}54.801'$, $24^{\circ}31.925'$ for SK-110-1 and $38^{\circ}54.840'$, $24^{\circ}31.885'$ for SK-121-a (see also Supplementary Table S1). Eight polished thin sections were prepared from the two collected samples.

Thin sections of samples SK-121-a and SK-110-1 were analyzed through a Leica microscope at the Università degli Studi di Milano-Bicocca for petrographic observations. The thin sections were carbon coated and subjected to Electron Probe Micro-Analysis (EPMA) with the JEOL 8200 Superprobe™ at the Università degli Studi di Milano, with a 15 kV accelerating voltage, a 5 nA beam current, and a 3 μm beam diameter.

5.2. PT pseudosection Modelling

We used the bulk-rock compositions of two rocks as proxies for representative samples from the upper (sample SK-110b) and the lower (sample SK-51) tectonic unit from Skyros island. PT pseudosections were calculated in the system SiO_2 – TiO_2 – Al_2O_3 – FeO – MgO – CaO – Na_2O – K_2O (H_2O as saturated phase component), employing *Perple_X* software (ver. 6.9.1; 2020) [39–41]. The thermodynamic database of Holland and Powell (1998; updated in 2004) was applied [42]. The solution models we used during calculation of the pseudosections were the following: *Bio(HP)* for biotite [43], *Carp(M)* for carpholite [44], *Chl(HP)* for chlorite [43], *Ctd(HP)* for chloritoid [43], *Gt(HP)* for garnet [43], *Pheng(HP)* for K-white mica [43], *Mica(M)* for paragonite [44], *Sud(M)* for sudoite [44], *Pu(M)* for pumpellyite [44], *Act(M)* for amphibole [44], *Stlp(M)* for stilpnomelane [44], *Omph(GHP)* for clinopyroxene [45], *Ep(HP)* for epidote [43], *MtUl(A)* for magnetite [46], *IlGkPy* for ilmenite, and feldspar for plagioclase [47]. The bulk-rock compositions based on whole-rock analysis, and thus the derived phase assemblage, are assumed to represent equilibrium over the scale of a hand specimen. However, since the analyzed rocks are fine-grained, then the analyzed composition can be regarded as the “effective” one (the composition that suggests grain-scale equilibrium). In this study, however, the calculated pseudosections, combined with the observed textural relations and mineral modal/chemistry data, provide a unique frame of P-T conditions for a specific bulk-rock composition, and also are a good proxy to derive the peak and post-peak stages along the metamorphic evolution [48]. *WERAMI* software (ver. 6.9.1) was used to compute isopleths for end-members of solid solutions. Finally, *PyWERAMI* software (Lexa, updated 2011) was used for calculation of selected mineral isopleths. After that, we exported each *PyWERAMI* plot to EPS format, and imported it into *CorelDraw* software (ver. X8).

5.3. $^{40}Ar/^{39}Ar$ Dating

For $^{40}Ar/^{39}Ar$ analyses, samples were irradiated in the McMaster University nuclear reactor (Ontario, Canada), carefully avoiding Cd shielding. The age monitor was hornblende MMhb1 with an assumed age of 523.1 Ma [49]. $^{40}Ar/^{39}Ar$ analyses followed the step-heating procedure described in [50] with the *NuInstruments™ Noblesse®* noble gas mass spectrometer at the Università degli Studi di Milano-Bicocca.

6. Results

Optical microscopy (Figure 6) reveals a main foliation defined by muscovite and minor chlorite, predated by a relict white mica oriented at a high angle to the foliation.

EPM analyses (Supplementary Table S1) quantify the composition of the main mineral phases. Both SK-121-a and SK-110-1 have very similar characteristics. Backscattered electron images (BSE; Figure 7) show that garnet, biotite, phengite, and chlorite \pm rutile \pm paragonite predate the main foliation, and are preserved as relicts (Figures 6b and 7b). Quartz recrystallized (Figure 6d,e) showing evidence of a bulging [51] recrystallization mechanism. Compositional diagrams (Figure 8a,b) of the texture and microstructure clearly detected white mica generations; they appear at first sight to suggest that these two generations of muscovite are chemically identical. As this is petrologically impossible (muscovite and phengite form at very different pressures), these two apparently contradictory observations can be explained as a grain size artefact. As the primary electron beam had a diameter of 3 μm , any microstructure finer than the beam will be confused with the surrounding matrix and give a meaningless average composition. This effect had been clearly documented by [52] on the four white mica generations that had remained in petrologic (and hence isotopic) disequilibrium in a high-grade gneiss. What is evident from the combination of imaging and quantitative analyses on selected spots is that one generation of white mica is HP phengite and one generation is retrograde muscovite (Figures 6 and 7).

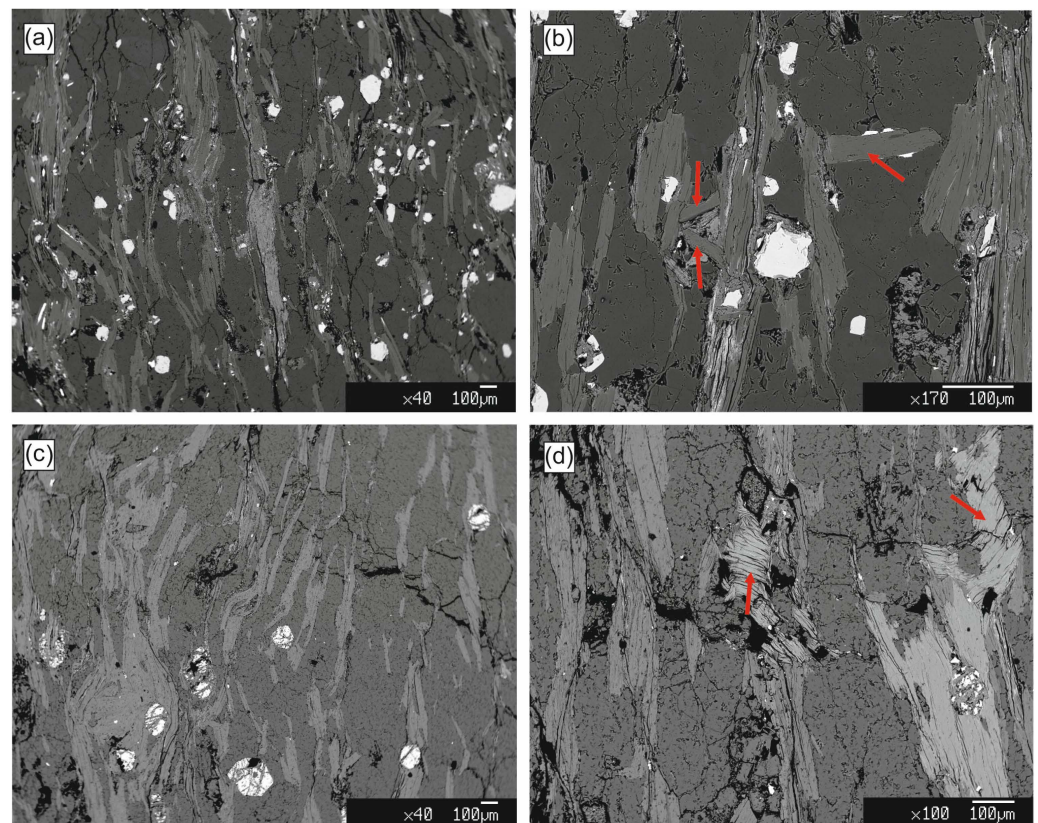


Figure 7. BSE images of sample thin sections. (a) BSE image of the SK-121-a sample. Muscovite makes the main foliation. (b) Relicts of muscovite are transversal to the foliation. Red arrows show the muscovite relicts (SK-121-a). (c) BSE image of the SK-110-1 sample. The main foliation is defined by muscovite. (d) Chlorite relicts (SK-110-1) are embedded in the main muscovite foliation. Red arrows show the chlorite (light gray).

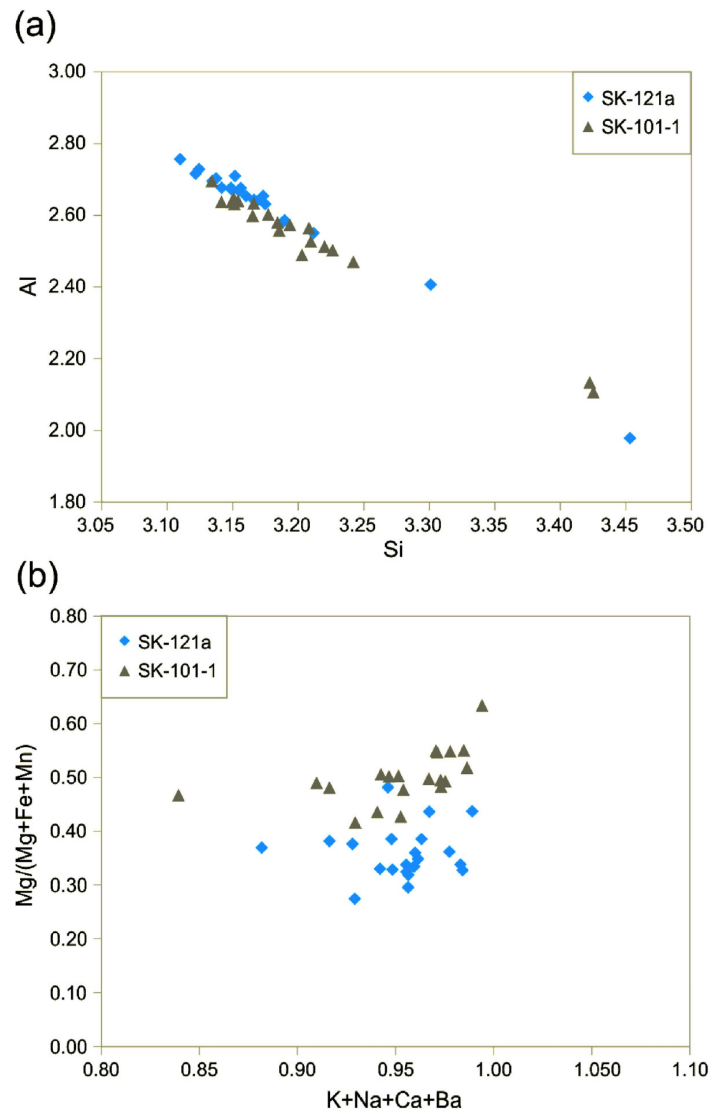


Figure 8. Electron Probe Micro-Analysis compositional diagrams of muscovite grains. (a) Al vs. Si diagram. Al and Si are shown as apfu (atoms per formula unit). Subordinate relicts of phengite ($\text{Si} \geq 3.45$ apfu) are distinct from the foliation-forming muscovite ($\text{Si} \leq 3.09$). (b) $\text{Mg}/(\text{Mg} + \text{Fe} + \text{Mn})$ vs. alkali sum. Most point analyses show an alkali content between 0.90 and 1.00, suggesting alteration $< 10\%$, i.e., moderate. The Mg/Fe ratio varies by a factor 2, which is strong evidence of very finely intergrown white mica generations of very different compositions.

Additional support for the occurrence of such an artefact comes from the spot electron probe microanalyses on two grains petrographically identified as paragonite in sample SK-101-1. The molar Na/Ca ratio is constant (22 ± 1); however, the apparent absolute concentrations vary by a factor of 2. This can only be explained as a sub- μm intergrowth of paragonite with a heterochemical, K-rich, Ca + Na-poor white mica.

The alkali content reveals the degree of ideality of micas, which can lose the interlayer cations by alteration. The sum of alkali cations (plus minor amounts of interlayer Ca and Ba) of the analyzed muscovite should be 1.00 apfu (atoms per formula unit) by stoichiometry. The measured spots mostly are higher than 0.90 apfu, meaning that alteration mostly was below 10% (Figure 8b).

The complete $^{40}\text{Ar}/^{39}\text{Ar}$ results are given in Supplementary Table S2. Rock samples of SK-121-a and SK-110-1 were crushed and sieved, and micas in the 125–250 μm fraction were separated by a Frantz™ Magnetic Separator at the Università degli Studi di Milano-Bicocca.

Muscovite crystals were then selected by handpicking under a stereomicroscope, avoiding impurities and contamination.

Any attempt to interpret their significance must take into account two facts: (1) the studied samples consist of a mixture of at least two different white mica generations that were formed at different P-T, and therefore at different times; mixtures should be unraveled following [53], making the best possible use of Ar isotope systematics. (2) As the scale at which the mica generations are intergrown is $<3 \mu\text{m}$ (as demonstrated by our EPMA observations), there are only two ways to date the individual mica generations: (2.1) degas a sample volume $\ll 1 \mu\text{m}^3$ to be sure to degas only one monomineralic species; however, the presently available mass spectrometers are not able to achieve sufficient precision on sub-attomole Ar concentrations accumulated in such an extremely small volume of a Phanerozoic mineral; (2.2) exploit the differential release of Ar from the respective crystal structures [54]. The latter option is discussed by [53,55,56].

7. Discussion

7.1. Late Cretaceous Ages in the UMU

The age spectra of the SK-121-a and SK-110-1 white mica separates are very similar: step ages increase from ca. 70 Ma to ca. 96 Ma (Figure 9a). An age spectrum alone is not conducive to reliable insight and can even be grossly misleading [55]. What provides clearer insight are the common-denominator isotope correlation diagrams [55,57], which show similar trajectories for the two samples (Figure 9b,c).

These trajectories bear petrogenetic information, as both the Cl/K and Ca/K ratios are powerful indicators of mineralogical identity and therefore of petrogenetic conditions (Ref. [58] and references therein). As detailed in the literature (e.g., Ref. [55] and references therein) mixtures are unraveled by identifying the endpoints of mixing trends. If all heating steps define a linear trend, then the system may be a binary mixing (or a two-dimensional projection of a three-dimensional point distribution indicating multiple mixing); if points deviate from a straight line, then at least one (or more) additional mixing end-members are required by simple mathematics.

The age vs. Cl/K common denominator isotope correlation diagram (Figure 9b) shows that both samples define a Z-shaped trajectory, starting with step 1 (lowest furnace temperature) at the lower right, climbing towards the left, then turning sharply towards the upper right at step 3, climbing further until step 9, and finally veering towards the upper left; step 11 of sample SK-110-1 adds a rightward shift to the Z-shaped trajectory (possibly very minute amounts of apatite, which has high Ca and at the same time high Cl concentrations). The age vs. Ca/K diagram starts with step 1 at the bottom right, climbs with a shallow slope until step 3, then climbs steeply towards the right until step 8, and finally veers with a shallow slope towards the right.

In both diagrams, the most parsimonious number of required endmembers is four. Two of them are related to alteration and/or xenocrystals having a high Ca/K ratio that rules them out as micas. Two white mica generations are indicated by Ar systematics, confirming the microtextural observations. The two schist samples are strictly related and have very similar degassing patterns. To infer the age of each population, we exploit the information provided by the composition vs. age diagrams (Figure 9b,c). The relict mica generation of sample SK-110-1 has a minimum age given by step 9 (the endpoint of the Cl/K–age correlation trend having the low Ca/K signature), i.e., $t \geq 93.5$ Ma. The same criterion applied to SK-121-a gives $t \geq 91.5$ Ma. The younger mica generation of SK-121-a, corresponding to step 3 (for which the Cl/K ratio is lowest), is inferred to have an age of approximately 78 Ma. The phase(s) characterized by high Ca/K ratios in steps 1–2 of both samples reflect alterations dated as ≤ 71 Ma (sample SK-110-1) and ≤ 66 Ma (sample SK-121-a). Comparing both samples, we propose that the main foliation was formed in the Late Cretaceous (ca. 78 Ma), preceded by relict mica ≥ 93.5 Ma, and followed by alteration ≤ 66 Ma. This alteration could be as young as Eocene (if it is subordinate by

mass balance), an age well documented as being a retrogression age across much of the Southern Aegean.

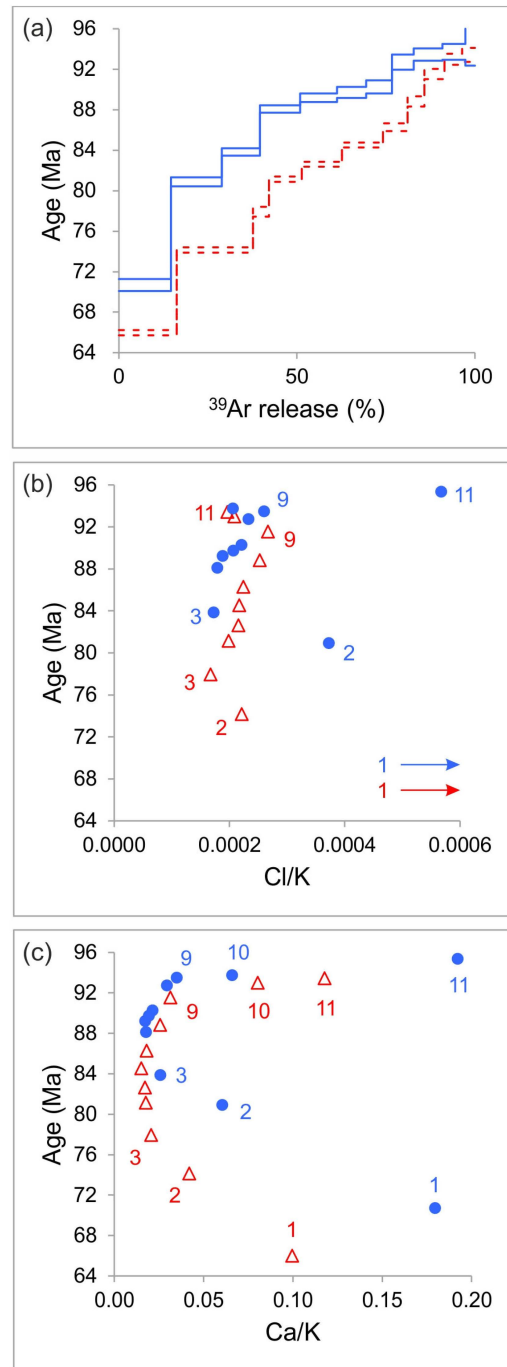


Figure 9. $^{40}\text{Ar}/^{39}\text{Ar}$ results for the analyzed samples. (a) Age spectra. SK-121-a (dashed lines) and SK-110-1 (continuous lines). All uncertainties are shown as 2σ . (b) Age vs. Cl/K common-denominator correlation diagram for SK-121-a (open triangles) and SK-110-1 (filled circles). Steps are numbered from 1 to 11; step 1 of both samples plots outside the boundaries and is marked by an arrow. The data are given in Table S2. The regular trajectory of the points from the lowest temperature steps to the highest temperature steps has a Z shape, which requires that four different phases were distinct Ar reservoirs. (c) Age vs. Ca/K common-denominator correlation diagram. The trajectory of the data points differs from that in (b), but its U shape requires the same four distinct Ar reservoirs degassed in the same temperature steps as (b).

7.2. Tectonic Implications

Based on its pelagic nature and its thrusting on the LMU and the Ophiolites, the UMU of Skyros, cropping out in Olympus Mountain, probably represents a segment of the Axios/Vardar oceanic domain (H4 in Figure 1). Its paleogeographic position should be in the internal margin of H4 towards its transition to the more internal continental platform terrane of Paikon–Lesvos (H5 in Figure 1). It was probably involved in the late stages of the Paleo-Alpine orogenic phase, undergoing subduction, detachment from the subducting slab, and subsequent rapid exhumation within the Late Cretaceous volcanic arc of the Hellenides [1]. It is remarkable that the underlying LMU of Skyros is composed of pelagic meta-sediments with submarine basic volcanism, resembling pelagic/oceanic Maliac affinities [59]. It is characterized by low grade greenschist assemblages such as albite + white mica + chlorite + epidote + quartz + calcite + Fe-oxides [60]. In addition, the absence of garnet, biotite, and amphibole, which are present in the UMU of Skyros, shows the significant difference in the metamorphic grade between the two metamorphic units of Skyros. Thus, the LMU of Skyros corresponds to the pelagic/oceanic units (well-known from continental Greece) of Axios/Vardar origin, which have been subducted with the oceanic crust and subsequently have been obducted together with the ophiolites on the internal carbonate platform of the Pelagonian domain (Almopia or Sub-Pelagonian units of H3) [2,3,10,11]. This geotectonic process was accompanied in some cases by low-grade metamorphism, similar to that of the LMU of Skyros observed in ophiolite mélanges; in other cases, it is observable in the deformation with folding and shearing of the so-called schist/hornstein formations, without metamorphism [1,3,61]. In all cases, the paleo-tectonized units were covered by the non-metamorphosed sediments of the Late Cretaceous transgression, implying that the tectono-metamorphic events were pre-Cenomanian [2,8].

In the case of Skyros Island, our study showed that the non-metamorphosed Upper Cretaceous limestones and Eocene flysch are involved in the final Alpine thrusting, inter-fingering between the underlying paleo-tectonized units of the Sub-Pelagonian, the ophiolites and LMU and the overlying UMU. Thus, the Late Cretaceous age we obtained for the metamorphic foliation of the UMU marks a separate particular tectono-metamorphic event, absent from the other units of Skyros and generally from the Hellenides, with the exception of the sparse small Tertiary tectonic klippen (cited previously) in Crete and the Cyclades. Taking into account our results together with the previously cited references on the Paleo-Alpine orogenic events, we can distinguish, from the chronological point of view, the following stages:

- (i) A first tectonic phase with intra-oceanic subduction of an Axios/Vardar oceanic segment, which was imbricated with ophiolites and acquired low-grade metamorphism during the Late Jurassic–Early Cretaceous. This segment is the LMU.
- (ii) At a later stage, probably during the Early Cretaceous, this metamorphic unit was tectonically emplaced/obducted upon the Sub-Pelagonian carbonate platform and formed the Eo-Hellenic nappe. This process is typical of the Paleo-Alpine orogenic events.
- (iii) During the Late Cretaceous, the previously deformed area was transgressed, and shallow water carbonates were deposited, followed by Eocene flysch. At the same period, in another more internal domain of the orogenic arc, where the volcanic arc was formed, we have the Late Cretaceous metamorphic events of the UMU.
- (iv) During the Early Cenozoic, the UMU was tectonically emplaced at a shallow tectonic level together with the detached Upper Cretaceous sediments over the paleo-tectonized units (LMU and Sub-Pelagonian).

The key point is that during the deposition of the Upper Cretaceous limestones above the paleo-tectonized units, the UMU of Skyros was under metamorphic conditions characterized by PT conditions of 9.2 ± 1 kbar and 550 ± 30 °C.

The new finding of Late Cretaceous tectono-metamorphic ages in Skyros Island extends the occurrence of this event to the North Aegean Sea, from a geographical point of view, and to the Internal Hellenides, from a geodynamic point of view (terrane H4 in Figure 1). In all cases, the tectonic units bearing the Late Cretaceous tectono-metamorphic

event are found as tectonic klippen emplaced above different units during the Eocene orogenic events. The Asteroussia nappe is observed above the Pindos/Ethia nappe in Crete [17–19], the Anafi metamorphic klippen above the non-metamorphic Eocene flysch in Anafi Island, southern Cyclades [21,22], the Nikouria nappe above the metamorphic Amorgos Unit [20], the Akrotiri unit above the Northern Cyclades unit in Tinos [24], and the Vari unit above the Northern Cyclades unit in Southern Syros [23]. In the cases of Crete and Anafi Islands, the tectonic klippen are observed above non-metamorphic units overlying Eocene flysch formations of H2, whereas in the cases of Amorgos, Tinos, and Syros Islands, they overlie Cycladic metamorphic units of H2 metamorphosed during the Early Cenozoic. It is also relevant that in Crete and in Anafi Island, the Late Cretaceous tectono-metamorphic events are accompanied by Late Cretaceous granites. Thus, the previously reported Late Cretaceous tectono-metamorphic events in the External Hellenides (terrane H2 in Figure 1) have to be investigated in a new geotectonic scenario of a high temperature domain in the back-arc area of the evolving Hellenic arc in the area of the internal tectono-metamorphic belt of Rhodope [1,4]. Skyros Island is probably closer to the Late Cretaceous magmatic/volcanic zone than the previously studied areas in the External Hellenides domain in Crete and Cyclades, which could be far-travelled distant units, during the Eocene-Oligocene tectonism of the Alpine orogeny.

8. Conclusions

The new geochronological data from the Upper Metamorphic Unit (UMU) of Skyros Island show that the Late Cretaceous tectono-metamorphic events known from the South Aegean are also observed in the North Aegean area within the Internal Hellenides domain. The tectonic units recording the Late Cretaceous tectono-metamorphic events are always found as tectonic klippen on top of tectonic units that are either metamorphosed (LMU of Skyros, Northern Cyclades blueschists, and Amorgos unit) or non-metamorphosed (Anafi autochthon Eocene flysch and Pindos/Ethia unit). The occurrence of the Late Cretaceous tectono-metamorphic events also in the Internal Hellenides in the North Aegean proves that plate convergence with subduction of the Tethyan elements of the African plate is continuous from the Jurassic to the present. The dominant high-grade metamorphic characteristics of the Late Cretaceous klippen and their co-existence with granitic bodies (Asteroussia, Anafi) indicate their formation within the paleo-volcanic arc.

Supplementary Materials: The following supporting information can be downloaded at: <https://www.mdpi.com/article/10.3390/geosciences14030069/s1>, Table S1: Electron microprobe analyses (EPMA) of muscovite, biotite, chlorite, phengite and paragonite crystals (wt%) of the SK-121a and SK-110-1. Mineral formula based on 11 oxygens; Table S2: $^{40}\text{Ar}/^{39}\text{Ar}$ dating results of SK-121a and SK-110-1 muscovite crystals. All isotopes are shown in mL. Uncertainties are shown as 1σ .

Author Contributions: Conceptualization, D.P. and D.B.; methodology, D.B., D.P., G.B. and C.M.; validation, D.P.; formal analysis, D.B., G.B. and C.M.; investigation, D.B., D.P., G.B. and C.M.; resources, D.P.; data curation, D.B., G.B. and C.M.; writing—original draft preparation, D.B.; writing—review and editing, D.B., D.P., G.B. and C.M.; supervision, D.P.; project administration, D.P. All authors have read and agreed to the published version of the manuscript.

Funding: This research received no external funding.

Data Availability Statement: The original contributions presented in the study are included in the article and Supplementary Materials, further inquiries can be directed to the corresponding author.

Acknowledgments: The authors would like to thank Elisa Malinverno for supporting the analyses. Special thanks to V. Barberini for assisting with $^{40}\text{Ar}/^{39}\text{Ar}$ dating and A. Risplendente for the EPM analyses. We warmly thank Igor Villa for encouragement and support. I. Baziotis is acknowledged for his help in the geothermobarometry. We also warmly thank three anonymous reviewers for their comments which deeply improved the paper, and Editor Olivier for the editorial handling of the manuscript.

Conflicts of Interest: The authors declare no conflicts of interest.

References

- Papanikolaou, D. *The Geology of Greece*; Springer International Publishing: Cham, Switzerland, 2021; p. 340.
- Papanikolaou, D. Timing of tectonic emplacement of the ophiolites and terrane paleogeography in the Hellenides. *Lithos* **2009**, *108*, 262–280. [[CrossRef](#)]
- Papanikolaou, D. Tectonostratigraphic models of the Alpine terranes and subduction history of the Hellenides. *Tectonophysics* **2013**, *595*, 1–24. [[CrossRef](#)]
- Papanikolaou, D.; Bargathi, H.; Dabovski, C.; Dimitriu, R.; El-Hawat, A.; Ioane, D.; Kranis, H.; Obeidi, A.; Oaie, C.; Seghedi, A.; et al. TRANSMED Transect VII: East European Craton–Scythian Platform–Dobrogea–1B7 alkanides–Rhodope Massif—Hellenides–East Mediterranean–Cyrenaica. In *The TRANSMED Atlas: The Mediterranean Region from Crust to Mantle*; Cavazza, W., Roure, F., Spakman, W., Stampfli, G., Ziegler, P., Eds.; Springer: Heidelberg, Germany, 2004.
- van Hinsbergen, D.J.J.; Hafkenscheid, E.; Spakman, W.; Meulenkamp, J.E.; Wortel, R. Nappe stacking resulting from subduction of oceanic and continental lithosphere below Greece. *Geology* **2005**, *33*, 325–328. [[CrossRef](#)]
- Celet, P.; Ferriere, J. Les Hellenides internes: Le Pelagonien. *Eclogae Geol. Helv.* **1978**, *71*, 467–495.
- Sengor, A.M.C.; Yilmaz, Y.; Sungurlu, O. Tectonics of the Mediterranean Cimmerides: Nature and evolution of the western termination of Palaeo-Tethys. *Geol. Soc. London Spec. Publ.* **1984**, *17*, 77–112. [[CrossRef](#)]
- Brunn, J.H. Les zones helléniques internes et leur extension; Reflexions sur l’orogénèse alpine. *Bull. Soc. Géol. Fr.* **1960**, *S7-II*, 470–486. [[CrossRef](#)]
- Mercier, J. Étude Géologique des Zones Internes des Hellénides en Macédonie Centrale (Grèce): Contribution à L’étude du Métamorphisme et de L’évolution Magmatique des Zones Internes des Hellénides. Ph.D. Dissertation, Faculté des Sciences de l’Université de Paris, Paris, France, 1968.
- Jacobshagen, V.; Risch, H.; Roeder, D. Die eohellenische phase. Definition und Interpretation. *Z. Dtsch. Geol. Ge.* **1976**, *127*, 133–145.
- Vergely, P. Tectonique des Ophiolites Dans les Hellenides Internes. Consequences sur L’évolution des Regions Tethysiennes Occidentales. Ph.D. Dissertation, Université de Paris Sud, Paris, France, 1984.
- Vergely, P. Chevauchement vers l’Ouest et retrocarriage vers l’Est des ophiolites: Deux phases tectonique au cours du Jurassique supérieur—Eocretace dans le Hellenides internes. *Bull. Soc. Géol. Fr.* **1976**, *18*, 223–244.
- Altherr, R.; Schliestedt, M.; Okrusch, M.; Seidel, E.; Kreuzer, H.; Harre, W.; Lenz, H.; Wendt, I.; Wagner, G.A. Geochronology of high-pressure rocks on Sifnos (Cyclades, Greece). *Contrib. Mineral. Petrol.* **1979**, *70*, 245–255. [[CrossRef](#)]
- Andriessen, P.; Boelriik, N.; Hebeda, E.; Priem, H.; Verdumen, E.; Verschure, R. Dating of the events of metamorphism and granitic magmatism in the Alpine Orogen of Naxos (Cyclades, Greece). *Contrib. Mineral. Petrol.* **1979**, *69*, 215–225. [[CrossRef](#)]
- Schliestedt, M.; Altherr, R.; Matthews, A. Evolution of the Cycladic crystalline complex. Petrology, isotope geochemistry and geochronology. In *Chemical Transport in Metasomatic Processes*; Helgeson, H.C., SchuJing, R.D., Eds.; Springer: Utrecht, The Netherlands, 1987; pp. 76–94.
- Seidel, E.; Kreuzer, H.; Harre, W. A Late Oligocene/Early Miocene high pressure belt in the External Hellenides. *Geol. Jahrb. Hess.* **1982**, *E23*, 165–206.
- Lippolt, H.J.; Baranyi, I. Oberkretazische Biotit—und Gesteinsalter aus Kreta. *Neues Jahrb. Geol. Palaontol. Abh.* **1976**, *7*, 405–414.
- Seidel, E.; Okrusch, M.; Kreuzer, H.; Raschka, H.; Harre, W. Eo-Alpine metamorphism in the uppermost unit of the Cretan nappe system. Petrology and geochronology: Part 1. The Léndas Area (Asteroúsia Mountains). *Contrib. Mineral. Petrol.* **1976**, *57*, 259–275. [[CrossRef](#)]
- Seidel, E.; Okrusch, M.; Kreuzer, H.; Raschka, H.; Harre, W. Eo-alpine metamorphism in the uppermost unit of the Cretan nappe system. Petrology and geochronology: Part 2. Synopsis of high temperature metamorphism and associated ophiolites. *Contrib. Mineral. Petrol.* **1981**, *76*, 351–361. [[CrossRef](#)]
- Dürr, S.; Altherr, R.; Keller, J.; Okrusch, M.; Seidel, E. The median Aegean crystalline belt: Stratigraphy, structure, metamorphism, magmatism. In *Alps, Apennines, Hellenides. Geodynamic Investigations along Geotraverses by an International Group of Geoscientists*; Closs, H., Roeder, D.H., Schmidt, K., Eds.; Schweizerbart: Stuttgart, Germany, 1978; pp. 455–477.
- Reinecke, T.; Altherr, R.; Hartung, B.; Hatzipanagiotou, K.; Kreuzer, H.; Harre, W.; Klein, H.; Keller, J.; Geenen, E.; Boger, E. Remnants of a late Cretaceous high temperature belt on the island of Anafi (Cyclades, Greece). *Neues Jahrb. Fur Mineral. Abh.* **1982**, *145*, 157–182.
- Martha, S.O.; Dörr, W.; Gerdes, A.; Petschick, R.; Schastok, J.; Xypolias, P.; Zulauf, G. New structural and U–Pb zircon data from Anafi crystalline basement (Cyclades, Greece): Constraints on the evolution of a Late Cretaceous magmatic arc in the Internal Hellenides. *Int. J. Earth Sci.* **2016**, *105*, 2031–2060. [[CrossRef](#)]
- Soukis, K.; Stockli, D.F. Structural and thermochronometric evidence for multi-stage exhumation of southern Syros, Cycladic islands, Greece. *Tectonophysics* **2013**, *595*, 148–164. [[CrossRef](#)]
- Patzak, M.; Okrusch, M.; Kreuzer, H. The Akrotiri Unit on the island of Tinos, Cyclades, Greece, witness to a lost terrane of late Cretaceous age. *Neues Jahrb. Geol. Palaontol. Abh.* **1994**, *194*, 211–252. [[CrossRef](#)]
- Jacobshagen, V.; Matarangas, D. Skyros Island. In *Geological Map of Greece at scale 1/50,000*; IGME: Athens, Greece, 1983.
- Papanikolaou, D.; Royden, L. Disruption of the Hellenic arc: Late Miocene extensional detachment faults and steep Pliocene–Quaternary normal faults—Or what happened at Corinth? *Tectonics* **2007**, *26*, TC5003. [[CrossRef](#)]

27. Papanikolaou, D.; Nomikou, P.; Papanikolaou, I.; Lampridou, D.; Rousakis, G.; Alexandri, S. Active tectonics and seismic hazard in Skyros Basin, North Aegean Sea, Greece. *Mar. Geol.* **2019**, *407*, 94–110. [[CrossRef](#)]
28. Harder, H.; Jacobshagen, V.; Skala, W.; Arafteh, M.; Berndsen, J.; Hofmann, A. Geologische Entwicklung und Struktur der Insel Skyros, Nord-Sporaden, Griechenland. *Berl. Geowiss. Abh.* **1983**, *48*, 7–40.
29. Ktenas, C. Report on the geological research effected during 1928–1929. *Proc. Acad. Athens* **1930**, *5*, 92–107.
30. Jacobshagen, V.; Skala, W.; Wallbrecher, E. Alpine structure and development of the southern Pelion peninsula and the North Sporades. In *Alps, Apennines, Hellenides. Geodynamic Investigations along Geotraverses by an International Group of Geoscientists*; Closs, H., Roeder, D.H., Schmidt, K., Eds.; Schweizerbart: Stuttgart, Germany, 1978; pp. 484–488.
31. Jacobshagen, V.; Wallbrecher, E. Pre-Neogene nappe structure and metamorphism of the North Sporades and the southern Pelion peninsula. *Geol. Soc. London Spec. Publ.* **1984**, *17*, 591–602. [[CrossRef](#)]
32. Papastamatiou, J. Quelques observations sur la géologie et la métallogénie de l'île de Skyros. *BGSG* **1961**, *1*, 219–237.
33. Philippson, A. Beiträge zur Kenntnis der griechischen Inselwelt. *Peterm. Mitt. Ergänzungsheft* **1901**, *134*, 1–172.
34. Boundi, D.; Papanikolaou, D. Differentiation of the structural fabric of the Skyros tectonic units from the Paleo-Alpine to the Alpine orogenic events. In Proceedings of the 16th International Congress of the Geological Society of Greece, Patras, Greece, 17–19 October 2022.
35. Whitney, D.L.; Evans, W. Abbreviations for names of rock-forming minerals. *Am. Mineral.* **2010**, *95*, 185–187. [[CrossRef](#)]
36. Boundi, D.; Baziotis, I.; Berndt, J.; Klemme, S. P-T constraints on upper and lower metamorphic unit rocks from Skyros Island. In Proceedings of the 16th International Congress of the Geological Society of Greece, Patras, Greece, 17–19 October 2022.
37. Boundi, D. Deciphering Alpine from Paleo-Alpine Events and Intergration of the Skyros Tectonic Units to the Geodynamic and Paleogeographic Frame of the Hellenides. Ph.D. Dissertation, University of Athens, Athens, Greece, 2024.
38. Kouketsu, Y.; Mizukami, T.; Mori, H.; Endo, S.; Aoya, M.; Hara, H.; Nakamura, D.; Wallis, S. A new approach to develop the Raman carbonaceous material geothermometer for low-grade metamorphism using peak width. *Isl. Arc* **2014**, *23*, 33–50. [[CrossRef](#)]
39. Connolly, J.A.D. Multivariable phase diagrams: An algorithm based on generalized thermodynamics. *Am. J. Sci.* **1990**, *290*, 666–718. [[CrossRef](#)]
40. Connolly, J.A.D. Computation of phase equilibria by linear programming: A tool for geodynamic modeling and its application to subduction zone decarbonation. *Earth Planet. Sci. Lett.* **2005**, *236*, 24–541. [[CrossRef](#)]
41. Connolly, J.A.D. The geodynamic equation of state: What and how. *Geochem. Geophys. Geosystems* **2009**, *10*, Q10014. [[CrossRef](#)]
42. Holland, T.J.B.; Powell, R. An internally consistent thermodynamic data set for phases of petrological interest. *J. Metamorph. Geol.* **1998**, *16*, 309–343. [[CrossRef](#)]
43. Powell, R.; Holland, T. Relating formulations of the thermodynamics of mineral solid solutions; activity modeling of pyroxenes, amphiboles, and micas. *Am. Mineral.* **1999**, *84*, 1–14. [[CrossRef](#)]
44. Massonne, H.-J.; Willner, A.P. Phase relations and dehydration behaviour of psammopelite and mid-ocean ridge basalt at very-low-grade to low-grade metamorphic conditions. *Eur. J. Mineral.* **2008**, *20*, 867–879. [[CrossRef](#)]
45. Green, E.; Holland, T.; Powell, R. An order-disorder model for omphacitic pyroxenes in the system jadeite-diopside-hedenbergite-acmite, with applications to eclogitic rocks. *Am. Mineral.* **2007**, *92*, 1181–1189. [[CrossRef](#)]
46. Andersen, D.J.; Lindsley, D.H. Internally consistent solution models for Fe-Mg-Mn-Ti oxides; Fe-Ti oxides. *Am. Mineral.* **1988**, *73*, 714–726.
47. Fuhrman, M.L.; Lindsley, D.H. Ternary-feldspar modeling and thermometry. *Am. Mineral.* **1988**, *73*, 201–215.
48. Baziotis, I.; Tsai, C.-H.; Ernst, W.G.; Jahn, B.-M.; Iizuka, Y. New P–T constraints on the Tamayen glaucophane-bearing rocks, eastern Taiwan: Perple_X modelling results and geodynamic implications. *J. Metamorph. Petrol.* **2017**, *35*, 35–54. [[CrossRef](#)]
49. Renne, P.R.; Swisher, C.C.; Deino, A.L.; Karner, D.B.; Owens, T.L.; De Paolo, D.J. Intercalibration of standards, absolute ages, and uncertainties in $^{40}\text{Ar}/^{39}\text{Ar}$ dating. *Chem. Geol.* **1998**, *145*, 117–152. [[CrossRef](#)]
50. Bosio, G.; Malinverno, E.; Villa, I.M.; Di Celma, C.; Gariboldi, K.; Gioncada, A.; Barberini, V.; Urbina, M.; Bianucci, G. Tephrochronology and chronostratigraphy of the Miocene Chilcatay and Pisco formations (East Pisco Basin, Peru). *Newsl. Stratigr.* **2020**, *53*, 213–247. [[CrossRef](#)]
51. Passchier, C.W.; Trouw, R.A.J. *Microtectonics*; Springer: Berlin, Germany, 2005.
52. Heri, A.R.; Robyr, M.; Villa, I.M. Petrology and geochronology of the “muscovite standard” B4M. In $^{40}\text{Ar}/^{39}\text{Ar}$ Dating: From Geochronology to Thermochronology, from Archaeology to Planetary Sciences; Jourdan, F., Mark, D., Verati, C., Eds.; Geological Society, London, Special Publications: London, UK, 2014; Volume 378, pp. 69–78.
53. Villa, I.M.; Hanchar, J.M. Age discordance and mineralogy. *Am. Mineral.* **2017**, *102*, 2422–2439. [[CrossRef](#)]
54. Montemagni, C.; Villa, I.M. Geochronology of Himalayan shear zones: Unravelling the timing of thrusting from structurally complex fault rocks. *J. Geol. Soc. London* **2021**, *178*, 1–13. [[CrossRef](#)]
55. Villa, I.M. The in vacuo release of Ar from minerals: 1. hydrous minerals. *Chem. Geol.* **2021**, *564*, 120076. [[CrossRef](#)]
56. Villa, I.M. Dating deformation: The role of atomic-scale processes. *J. Geol. Soc. London* **2022**, *179*, jgs2021-098. [[CrossRef](#)]
57. Villa, I.M. Radiogenic isotopes in fluid inclusions. *Lithos* **2001**, *55*, 115–124. [[CrossRef](#)]
58. Bosse, V.; Villa, I.M. Petrochronology and hygrochronology of tectono-metamorphic events. *Gondwana Res.* **2019**, *71*, 76–90. [[CrossRef](#)]

59. Ferrière, J. Sur la signification de séries du massif d'Othris (Grèce continentale centrale): La zone isopique maliaque. *Ann. Soc. Geol. Nord.* **1976**, *96*, 121–134.
60. Baltatzis, E. Distribution of elements between coexisting phengite and chlorite from low grade rocks from Skyros island, Greece. *Mineral. Petrol.* **1988**, *37*, 293–303.
61. Mercier, J.; Vergely, P. Les mélanges colorés (colored mélanges) de la zone d' Almopias (Macedoine, Grece). *CR Somm. Soc. Géol. Fr.* **1972**, 70–73.

Disclaimer/Publisher's Note: The statements, opinions and data contained in all publications are solely those of the individual author(s) and contributor(s) and not of MDPI and/or the editor(s). MDPI and/or the editor(s) disclaim responsibility for any injury to people or property resulting from any ideas, methods, instructions or products referred to in the content.